



Science Arts & Métiers (SAM)

is an open access repository that collects the work of Arts et Métiers Institute of Technology researchers and makes it freely available over the web where possible.

This is an author-deposited version published in: <https://sam.ensam.eu>
Handle ID: <http://hdl.handle.net/10985/10836>

To cite this version :

Mohammadali SHIRINBAYAN, Benjamin SUROWIEC, Michel BOCQUET, Abbas TCHARKHTCHI, Joseph FITOUSSI, Fodil MERAGHNI - Micro and macroscopic characterization of A-SMC under high speed tensile test - 2015

Any correspondence concerning this service should be sent to the repository

Administrator : scienceouverte@ensam.eu



MICRO AND MACROSCOPIC CHARACTERIZATION OF A-SMC UNDER HIGH SPEED TENSILE TEST

M. Shirinbayan ¹, J. Fitoussi ¹, F. Meraghni ², B. Surowiec ³, M. Bocquet ¹ and A. Tcharkhtchi ¹

¹Arts et Métiers ParisTech, PIMM – UMR CNRS 8006,
151 Boulevard de l'Hôpital, 75013 Paris, France

Emails: mohammadali.shirinbayan@ensam.eu; joseph.fitoussi@ensam.eu; michel.bocquet@ensam.eu;
abbas.tcharkhtchi@ensam.eu, web page: <http://pimm.paris.ensam.fr>

²Arts et Métiers ParisTech, LEM3 – UMR CNRS 7239,
4 Rue Augustin Fresnel, 57078 Metz, France

Email: fodil.meraghni@ensam.eu, web page: <http://www.lem3.fr>

³PLASTIC OMNIUM AUTO EXTERIOR SERVICES, Sigmatech, Sainte Julie, France

Email: benjamin.surowiec@plasticomnium.com, web page: <http://www.plasticomnium.com/fr/>

Keywords: A-SMC; Glass fibers; High strain rate; Fiber/matrix bond; Delamination

ABSTRACT

Advanced Sheet Molding Compound (A-SMC) is a serious composite material candidate for structural automotive parts. It has a thermoset matrix and consists of high weight content of glass fibers (50% in mass) compared to standard SMC with less than 30% weight fiber content. During crash events, structural parts are heavily exposed to high rates of loading and straining. This work is concerned with the development of an advanced experimental approach devoted to the micro and macroscopic characterization of A-SMC mechanical behavior under high-speed tension. High speed tensile test are achieved using servo-hydraulic test equipment in order to get required high strain rates up to 100 s⁻¹. Local deformation is measured through a contactless technique using a high speed camera. Numerical computations have led to an optimal design of the specimen geometry and the experimental damping systems have been optimised in terms of thickness and material properties. These simulations were achieved using ABAQUS explicit finite element code. The developed experimental methodology is applied for two types of A-SMC: Randomly Oriented fibers (RO) and Highly Oriented fibers (HO) plates. In the case of HO samples, two tensile directions were chosen: HO-0° (parallel to the Mold Flow Direction (MFD)) and HO-90° (perpendicular to the MFD). High speed tensile tests results show that A-SMC behavior is strain-rate dependent although the young's modulus remains constant with increasing strain rate. In the case of HO-0°, the stress damage threshold is shown an increase of 63%, when the strain rate varies from quasi-static (0.001 s⁻¹) to 100 s⁻¹.

1 INTRODUCTION

Sheet Molding Compounds (SMCs) are high strength glass reinforced thermoset moulding materials processed by thermo-compression [1]. SMC composites combine glass fiber and unsaturated polyester/phenolic/Vinyl and Acrylic modified resins to produce a high strength moulding compound [2-5]. These materials are usually formulated to meet performance requirements of the part to be molded. Moreover, Vinyl-esters resins used for new Advanced SMCs (A-SMC) exhibit many desirable features, including mechanical properties comparable to those of epoxy, excellent chemical resistance and tensile strength, and cost competitiveness. Moreover, its low viscosity enables room-temperature infusion. SMC and A-SMC are ideal for large structural automotive components because of their high strength-to-weight ratio [6,7]. Due to significant tooling investment, overall component cost savings resulting from part consolidation, with the same coefficient of thermal expansion as steel and excellent corrosion resistance; A-SMC is an ideal alternative to metals and can be used in the same fluctuating temperature environments [8,9].

Mechanical response of SMC composites is sensitive to the rate at which they are loaded [10-13]. Hence, for the effective use of these composites, their response under different strain rates should be clearly understood. During experimental high speed tests, the composite is generally subjected to rapid accelerations. So, at the beginning of the loading many complex processes occur due to rapid straining coupled to inertial disturbances and test system ringing [12]. Spatio-temporal variations of the strain and stress fields during a high speed test make the analysis more difficult [12,14]. Due to these complicated experimental conditions, not enough reliable material data has been determined at typical crash speeds. In order to increase safety, reliable material properties at typical crash speeds are essential for precise simulations of crash processes involving composite parts [15-17].

A first study on a standard SMC composite reinforced with 30% glass fiber [12] showed that the elastic modulus remains insensitive to the load rate for the explored velocity range; from quasi-static to up to 200 s^{-1} , a rough average value of 13 GPa is found. However, the microstructure variability of this class of materials can bring about a slight discrepancy [10-12] notably for dynamic loadings. Several studies [8-12] showed that the predominant damage mechanism for standard SMC composites is the debonding at the fiber-matrix interface. An experimental methodology [12] based on dynamic tensile tests has contributed to emphasize the strain rate effects on the overall behavior of SMCR26 composites. It has been demonstrated that as the strain rate increased, a delayed damage onset is followed by a slightly reduced damage accumulation kinetic. The notion of visco-damaged behaviour due to the time-dependent fiber-matrix interface strength has been emphasized for this SMC composite. The results of this study have provided the experimental framework to identify and validate a multi-scale model integrating the material microstructure effects [8]. This model is currently implemented into a FE code [18].

In the present paper, an experimental study is carried-out to investigate the strain rate influence on the overall mechanical behavior of a new Advanced SMC. The organization of this work is as follow: after a presentation of the main physical characteristics and microstructure of A-SMC composite, an optimization of high speed tensile test until failure is proposed through finite element analysis using a commercial explicit code (ABAQUS explicit) in order to take into account the perturbations mentioned above. Two kinds of A-SMC microstructures are investigated: Randomly Oriented fibers (RO) and Highly Oriented fibers (HO). In the case of HO samples, two tensile directions were chosen in order to evaluate the anisotropic effect due to microstructure: HO-0° (parallel to the Mold Flow Direction (MFD)) and HO-90° (perpendicular to the MFD). Moreover, SEM fractography analysis emphasizes the effect of microstructure and strain rate on the main damage and failure micro-mechanisms. At the end of the paper, a special attention is given to the analysis of the pseudo-delamination occurring just before failure. The effect of microstructure and strain rate on the pseudo-delamination is studied.

2 EXPERIMENTAL INVESTIGATIONS

2.1 Material description and processing

Advanced Sheet Molding Compound composite (A-SMC) consists of high content of glass fibers (50% in mass corresponding to 38.5% in volume) in contrast to standard SMC containing a maximum of only 30% in mass of glass fiber. Standard SMC is classically used in automotive industry for semi-structural part like rear floor or inner panel of a tailgate for instance. A-SMC as a thermoset material is a serious candidate for structural parts (security parts).

A-SMC is a high mechanical performance SMC based on vinyl-ester resin and reinforced with high ratio of chopped bundles of glass fibers (25 mm length). The composition of A-SMC as a good choice for automotive industry is shown in Table 1. For the need of this study, two types of A-SMC plates have been provided by PLASTIC OMNIUM AUTO EXTERIOR SERVICES: Randomly Oriented (RO) and Highly Oriented (HO) plates. HO plates have been obtained by an initial charge put only in the left part of a rectangular mould ($30 \times 40 \text{ cm}$) before compression leading to material flow. RO plates were obtained without material flow by completely filling the mold.

Product nature	Composition (content in mass percent)
Glass fibers	50 %
Vinyl-ester resin	24 %
Filler	24 %
Other products	2 %

Table 1. A-SMC Composition

2.1.1 Microstructure

Microscopic observations and image analysis, using SEM, have been performed in the aim to investigate qualitatively the material microstructure and especially fibers orientation. Indeed, fibers are initially randomly oriented in the sheets plane before compression. The fibers are presented as bundles of constant length ($L = 25$ mm). Each bundle contains approximately 250 fibers of $15\text{ }\mu\text{m}$ diameter. Glass fibers weight content is of 50%. Fig. 1 shows microstructure of A-SMC composite which obtained on polished surfaces.

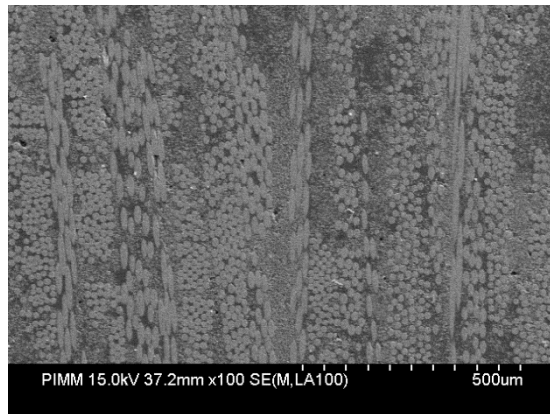


Fig. 1. Microstructure of A-SMC: Randomly oriented bundle of fibers

Fig. 2 represents the distribution of the fiber content in the RO and HO plates as a function of the cutting orientation. It can be assumed that, due to the flowing during molding process, most of the fibers remain on the plane of the plate and tend to be oriented parallel to the Mold Flow Direction (MFD).

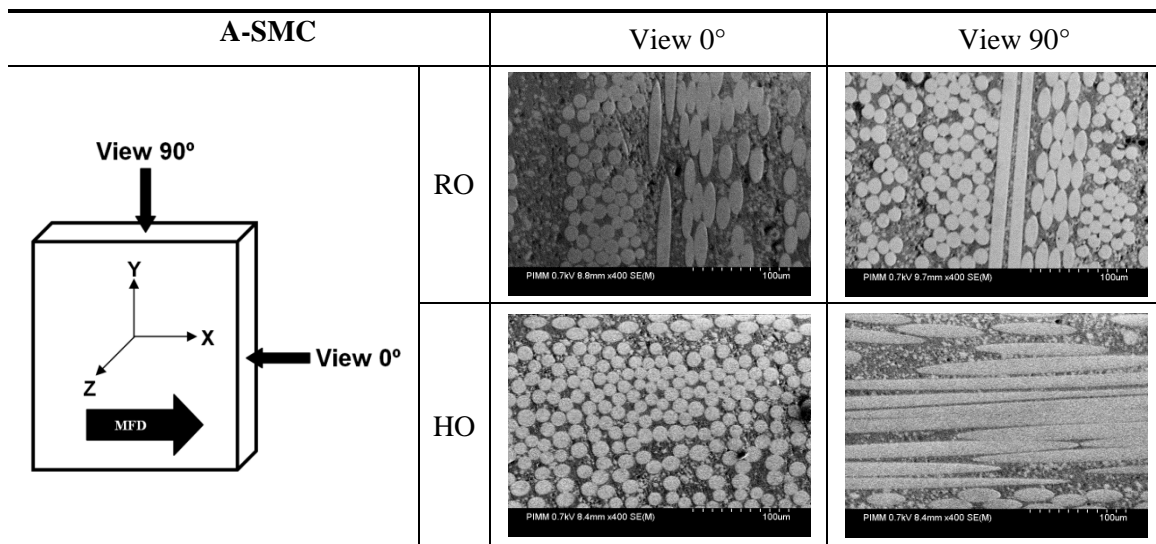


Fig. 2. Orientation of the fibers inside bundles in A-SMC

2.2 High-speed tensile tests

2.2.1 Testing devices

High-speed tensile tests have been conducted upon a servo-hydraulic test machine. As specified by the manufacturer (Schenk Hydropuls VHS 5020), the test machine can reach a crosshead speed range from 10^{-4} m/s (quasi-static) to 20 m/s. Moreover, the load level is measured by a piezoelectric crystal load cell having a capacity of a 50 kN. The test machine is equipped with a launching system. The composite specimen is positioned between the load cell (upper extremity) and the moving device (lower extremity) as sketched in Fig. 3.

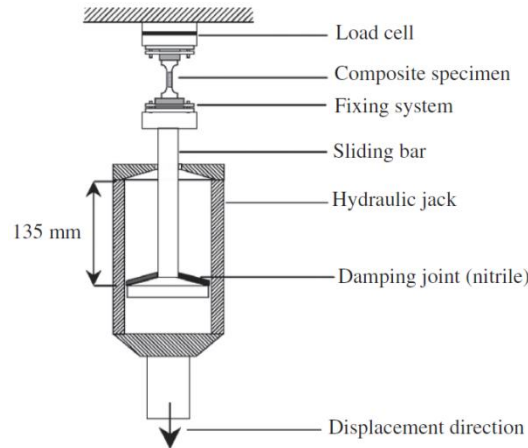


Fig. 3. Experimental device used for high-speed tensile tests

2.2.2 Optimization of high-speed tensile experiments

An optimal design of the damping joint, in terms of constitutive material and geometry, may result in a constant strain-rate and in homogeneous strain and stress fields in the central zone of the composite specimen. We have chosen a damping joint consisting of a low impedance material: rubber nitrile (1.5 mm thickness).

Specimen geometry has to be also optimised in order to reduce the perturbation wave's effect. The idea is to produce a reduction of the stress wave propagation occurring for a high-speed tensile test by mean of brutal variation of the specimen mechanical impedance. This variation of mechanical impedance leads to the trapping of the mechanical waves in the lower part of the testing device far from the specimen.

Therefore, the composite specimen geometry has been optimized as a result of numerical computations using ABAQUS finite element (FE) code. The criterion used for the optimization consists in reaching a stabilized strain distribution and strain rate within the specimen gauge section at the beginning of the loading stage.

On the basis of the FE simulations and assuming that the specimen behaves like an elastic anisotropic solid, a recursive optimization procedure results in the determination of optimal geometrical parameters: L_1 , L_2 , L_3 and R (see Fig. 4).

A-SMC		L_1 (mm)	L_2 (mm)	R (mm)	L_3 (mm)	L_4 (mm)
	1	20	2	5	10	20
	2	22	2	6	10	20
	3	25	2	7.5	10	20
	4	25	2	14	10	20

Fig. 4. Used specimen dimensions for the optimization methodology

Finally, the 6 mm radius specimen corresponds to the optimised geometry. Fig. 5 shows the spatio-temporal profiles of the longitudinal stress (σ_{11}) calculated along the central line of the optimized A-SMC specimen. It can be observed that the shock wave vanishes very quickly. Actually, the stress distribution becomes relatively homogeneous.

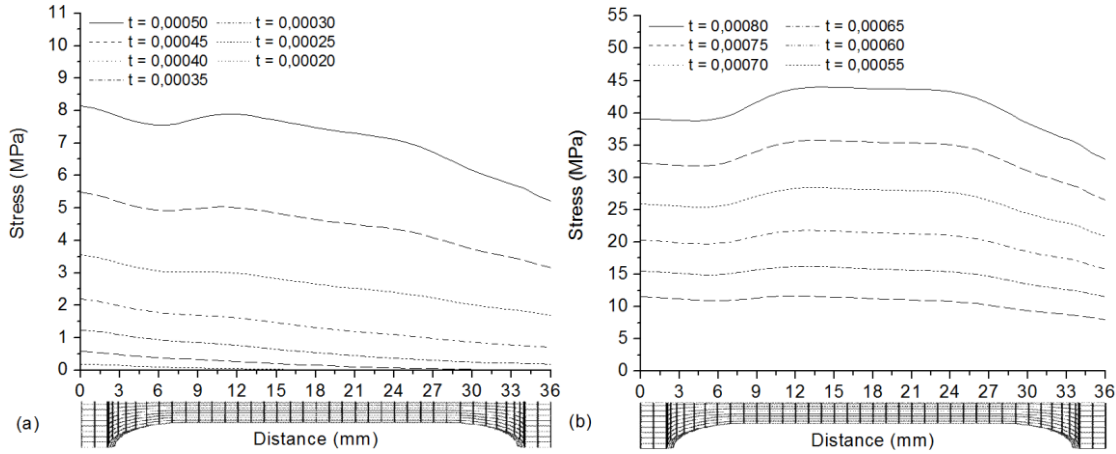


Fig. 5. Spatio-temporal profile of σ_{11} calculated along the central line of the A-SMC specimen. Loading conditions: imposed velocity $V = 4$ m/s. (a) First steps and (b) next steps

2.2.3 Strain and strain rate measurements

Local deformation is measured through a contactless technique using a high speed camera: two points were marked on the surface of the specimens defining the initial gauge length which is about 20 mm. A high speed camera (FASTCAM-APX RS) with the capacity 250000 frames per second was used to record pictures during high speed deformation. Image analysis is then used in order to follow the displacement of the centroid of each marked point to compute the evolution of the strain between the two points. After thresholding of the pictures, the evolution of the relative positions of the two points during deformation is computed. Then, strain measurement can be performed as shown in Fig. 6. One can note that after the damping stage characterized by a progressive increase of strain rate, the later becomes constant. Thus, strain rate can be easily determined from the slope of the linear part of the curve.

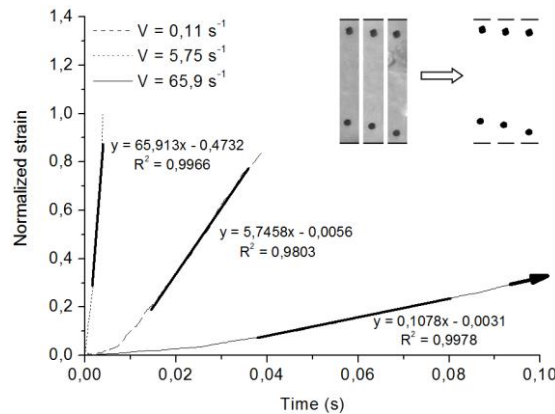


Fig. 6. Typical contactless strain measurements at various high strain rates

3 EXPERIMENTAL RESULTS AND DISCUSSION

3.1 Validation of the optimization procedure

Fig. 7 shows an example of strain evolution during a 2 m/s imposed velocity tensile test. Strain rate is stabilized after a measured rise time of about 1.3×10^{-4} s⁻¹. Moreover, it can be shown that at this time, the material still behaves elastically. Actually, the first non linearity is four time higher than the

tensile stress at equilibrium. Thus, it can be assumed that the equilibrium of the specimen is reached before the end of the yield strength. Thus, the measurement of the Young's modulus is reliable.

Moreover, a comparison between experimental and numerical evolution of the strain in the central zone of the specimen (obtained for the optimised geometry) is also shown in Fig. 7. A very good correlation is observed.

One can note that after 10^{-4} s, the strain rate is also stabilized and has a rough value of 60 s^{-1} . However, according to the finite elements calculations, the measured strain rate value is 40% less than the theoretical one (100 s^{-1}). As discussed above, this difference is due to inertial effects. On the basis of the very good agreement between the obtained experimental curves and numerical results, one can claim that our optimization procedure and the proposed geometry are validated.

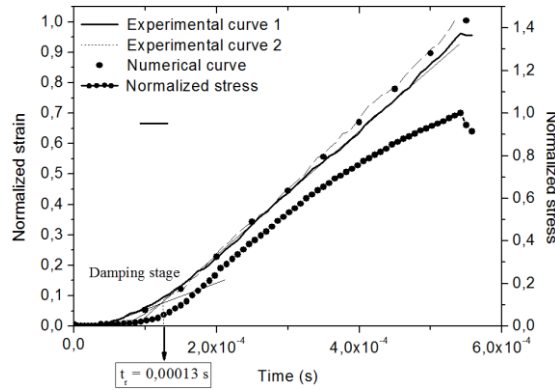


Fig. 7. Evolution of strain and stress in the central zone of the specimen; Comparison between experimental and numerical results obtained for the optimized geometry for A-SMC composites

3.2 High strain rate tensile curves

The stress-strain curves can be described by three stages:

- (i) Linear elastic behavior,
- (ii) Damage initiation corresponding to a knee point (apparition of a non-linear behavior),
- (iii) Damage propagation corresponding to a second linear stage.

In Fig. 8, stress-strain (σ - ϵ) tensile curves are plotted for several strain rates. Tensile curves obtained for RO, HO-90°, and HO-0° show clearly that the overall behavior is highly load-rate dependent. Indeed, under rapid tensile load, A-SMC composites exhibit typically a non-linear response. It should be indicated that, in these curves, the part concerning delamination phenomena was eliminated for favorable comparison.

Material mechanical characteristics have been estimated, as a function of strain rate. Fig. 8 show that initial slopes of the stress-strain curves are roughly identical for the range of tested strain rate values. Therefore, it means that the elastic modulus remains insensitive to strain rate. Young's moduli have a rough average value of 12, 14.5 and 18.5 GPa for HO-90°, RO and HO-0°, A-SMCs respectively.

3.3 Effects of strain-rate on the overall tensile response

Material characteristics, namely Young's modulus (E); damage thresholds corresponding to the first non-linearity ($\sigma_{\text{threshold}}$, $\epsilon_{\text{threshold}}$) and ultimate stress and strain (σ_{ultimate} , $\epsilon_{\text{ultimate}}$) are shown in Fig. 9 and Fig.10. Note that the ultimate characteristics correspond to the maximum stress level (before delamination when it occurs). Fig. 8 enables to emphasize that the material elastic modulus measured in the first stage of the stress-strain curve remain insensitive to the strain rate. However, the non-linear overall response of the A-SMC is drastically influenced by strain rate. Indeed, one can note that the damage threshold (Fig. 10), in terms of stress and strain, increases with strain rate. In fact, in the case of HO-0°, when varying the strain rate from the quasi-static to 100 s^{-1} , an increase of 63% of the stress damage threshold is shown. On the other hand, the ultimate stress shows an increase of 34%.

In accordance to results obtained on a standard SMC [12], as the strain rate increases, noticeable effects consist of a delayed damage onset (delay of the knee-point) and ultimate stress. It can be

established that the strain rate brings about a viscous nature of damage initiation and propagation. Like for standard SMC, A-SMCs also present a visco-damageable behavior. However, it must be noticed that, contrary to standard SMCs, the non-linear slope of the third stage of the A-SMCs curves (corresponding to the damage propagation stage) is also rate sensitive especially for RO A-SMC.

Moreover, one can notice that for all microstructure orientation, no significant strain rate effect is noticed on the ultimate strain.

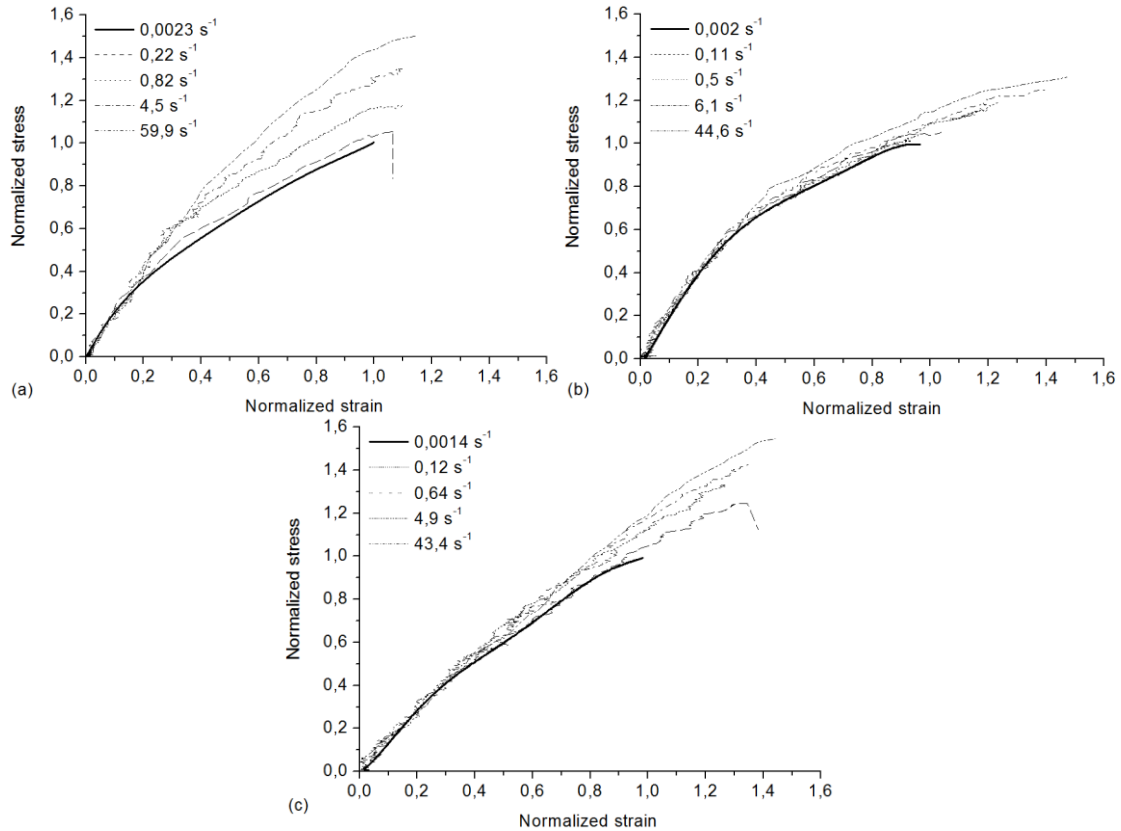


Fig. 8. Experimental high strain rate tensile curves
(Normalized stress (resp. strain) = stress (resp. strain) / ultimate stress (resp. strain)
obtained in quasi-static): (a) RO, (b) HO-90° and (c) HO-0°

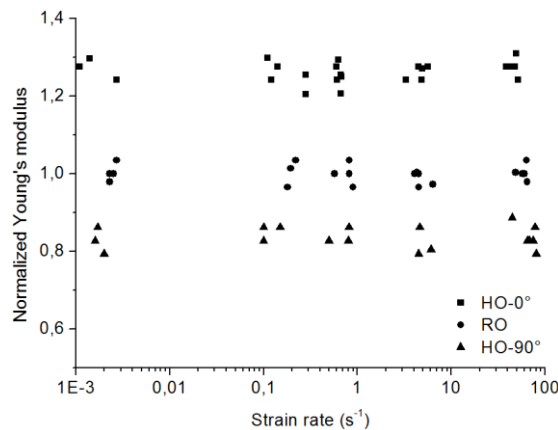


Fig. 9. Evolution of the normalized Young's modulus vs. strain rate
(Normalized Young's modulus = Young's modulus / average Young's modulus
obtained for quasi-static for RO-A-SMC)

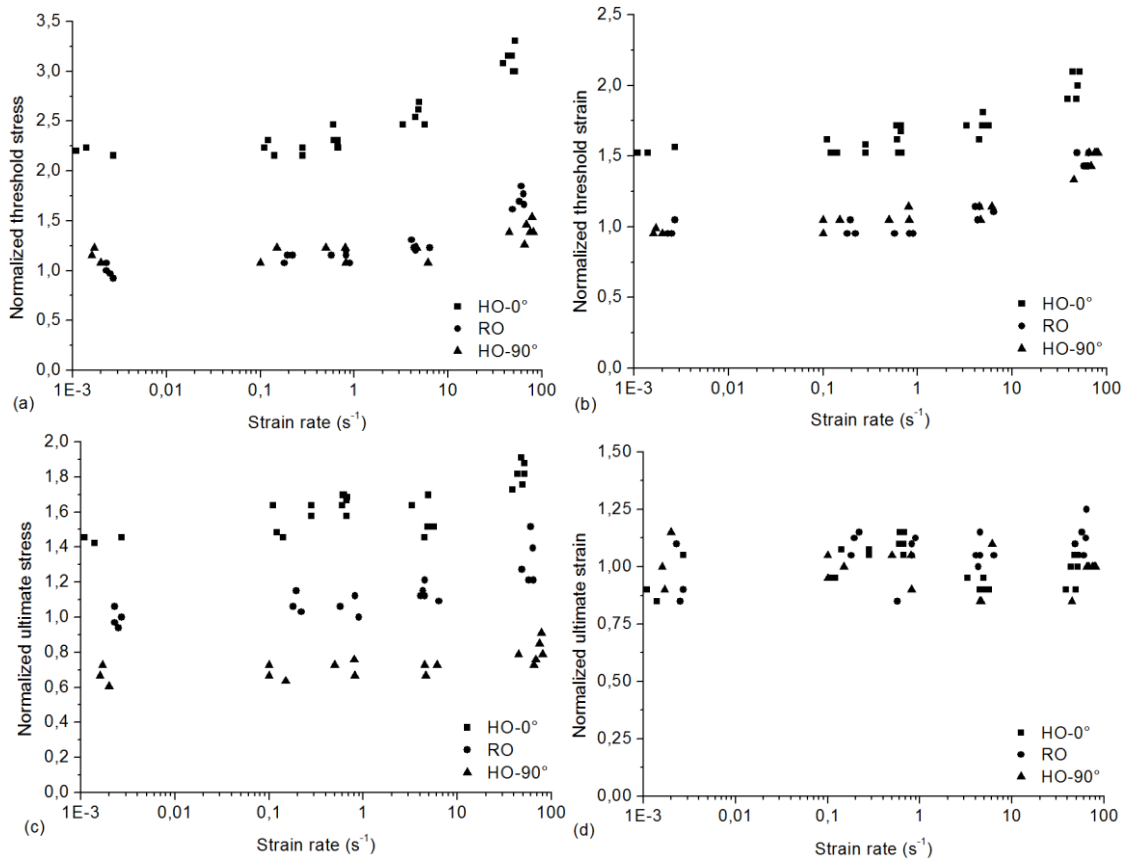


Fig. 10. Influence of strain rate: (a) Normalized threshold strain, (b) Normalized threshold stress, (c) Normalized ultimate strain and (d) Normalized ultimate stress (Normalized value = current value / average value obtained for quasi-static tests performed on RO-A-SMC)

3.4 Damage mechanisms investigation

In order to understand the physical origin of the damage delay, it is necessary to perform experimental investigations at the microscopic scale in order to identify the corresponding damage mechanisms.

The first investigations concerns quasi-static (0.5 mm/min) bending behavior performed on HO-A-SMC composite. In order to identify the influence of the microstructure on damage mechanisms occurring at the local scale, four points bending tests have been performed inside a SEM on HO-0° and HO-90° rectangular specimens. For both orientations, debonding at the fiber-matrix interface appears clearly to be the predominant damage mechanism. Interface debonding mostly appears on the fibers oriented orthogonally to the principal stress direction (90° oriented fibers) due to high local normal stresses at the interface. Coalescence of interface failure between adjacent fibers leads to localised transverse cracks appearing on several locations in the 90° oriented bundles. Propagation of these cracks into the matrix can also occur but the high content of fibers leads, in general, to the bifurcation of these cracks around surrounding more disoriented bundles of fibers. Then, pseudo-delamination between bundles is initiated. Fiber breakage can also appear at the end of the test just before failure. Interface debonding coupled to pseudo-delamination finally leads to failure by coalescence of the microcracks.

However, the thresholds of fiber-matrix interface damage and delamination are very dependant of the orientation of the sample. Fig. 11 shows for each orientation a first picture obtained at the initiation of the fiber-matrix interface debonding and a second one for the ultimate stress corresponding to pseudo-delamination just before failure. It has been shown that, for HO-0°, interface failure remains limited while pseudo-delamination is favored. On the other hand, when the fibers are oriented perpendicularly to the principal stress direction, pseudo-delamination is limited when fiber-matrix interface becomes predominant. Thus, it can be conclude that two principal mechanisms are in

competition: fiber-matrix interface debonding and pseudo-delamination. Moreover, the relative participation of each mechanism strongly depends on the orientation of the fibers.

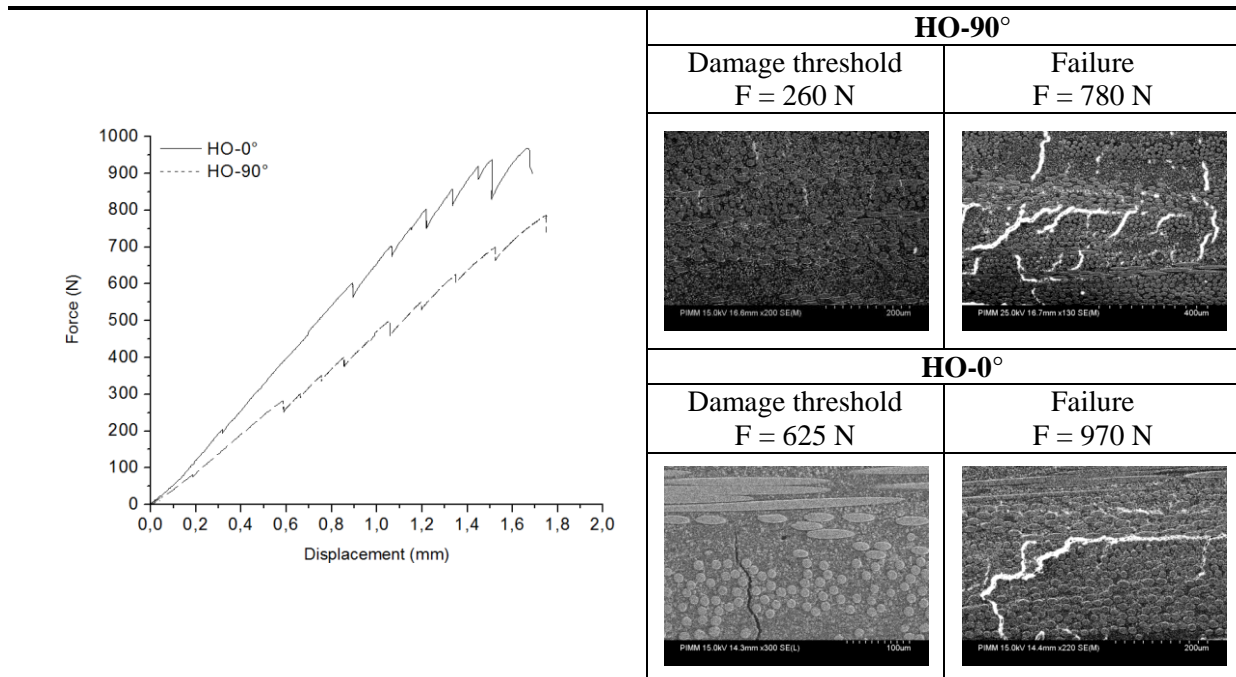


Fig. 11. Damage mechanisms under bending loading for HO-A-SMC composites

On the other hand, SEM observations have been performed on the fracture surfaces for tensile specimens for quasi-static and high strain rate (around 100 s^{-1}) loadings. Note that, in all micrographs shown after, the tensile direction corresponds to the horizontal direction.

SEM analysis performed on tensile specimens highlight the same damage mechanisms as shown in quasi-static bending test: fiber-matrix interface debonding and pseudo-delamination (see Fig. 12). These two mechanisms are observed for both quasi-static and dynamic tests regardless of the orientation of the bundles of fibers.

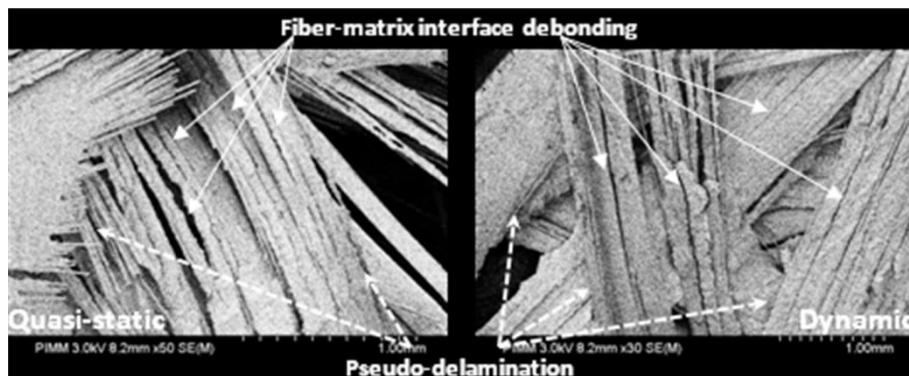


Fig. 12. Damage mechanisms for quasi-static and dynamic tensile tests*

Fig. 13(a), (b) and (c) show fiber-matrix interface debonding for 0° , 45° , and 90° oriented fibers relative to the tensile direction. One can notice that broken interfaces are always surrounded by pieces of matrix. This indicates high strength properties of the fiber-matrix interface for both quasi-static and dynamic loading.

In Fig. 14, it is noticeable to see that during pseudo-delamination, bundles of fibers are pulled out from each other simultaneously with breakage of the surrounding matrix. See also Fig.13 (b) for higher magnification.

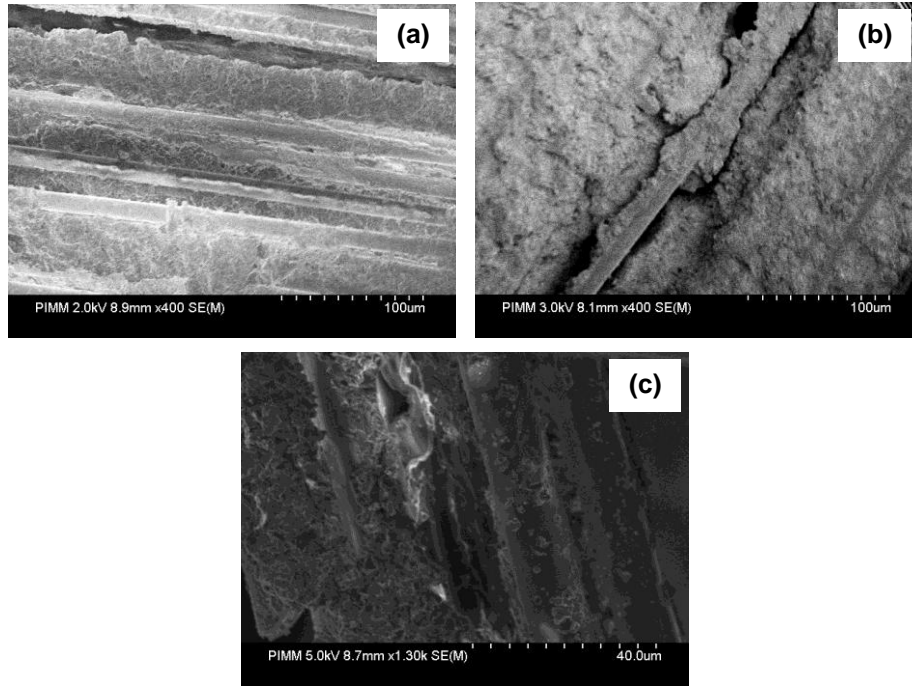


Fig. 13. Fiber-matrix interface debonding for several fiber orientation
(a) 0° (around 100 s⁻¹), (b) 45° (around 100 s⁻¹), (c) around 90° (quasi-static)

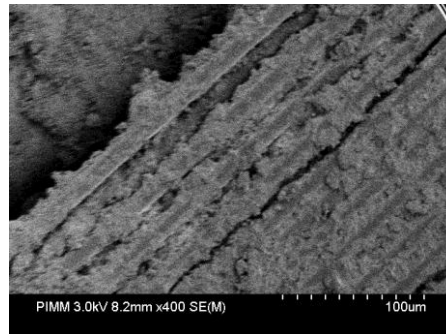


Fig. 14. Pseudo-delamination through surrounding matrix breakage

4 CONCLUSIONS

A-SMC is a high mechanical performance SMC based on vinyl-ester resin and reinforced with high content of glass fibers (> 50% weight content) compare to standard SMC (30% weight content). An original method for high strain rate testing optimization has been validated for moderate rates up to 100 s⁻¹. The developed experimental methodology based on dynamic tensile tests has contributed to emphasize the strain rate effects on the overall behavior of A-SMC composites. The strain rate is measured through a contactless technique using a high speed camera. Moreover, SEM micrographs show that most of the fibers are more or less oriented according to the disposition of the A-SMC prepreg and process parameters. In order to represent as well the structural response during a automotive crash, the strain rate effect on the mechanical behavior of two type of microstructure have been studied: Randomly Oriented fibers (RO) and Highly Oriented fibers (HO). Experimental results of high strain rate tensile tests show that the composite behavior is strongly strain-rate dependent although the Young's modulus remains constant for RO and HO samples when strain rate increases. On the contrary, as the strain rate increased, noticeable effects consist of a delayed damage onset: for example, the stress damage threshold of HO-0°-A-SMC showed an increase of 63% when increasing the strain rate from quasi-static (0.001 s⁻¹) to 100 s⁻¹. In the same time, a 40% increase of the ultimate stress can be observed when the ultimate strain does not seem to be significantly affected.

REFERENCES

- [1] Le TH, Dumont PJJ, Orgéas L, Favier D, Salvo L, Boller E. X-ray phase contrast microtomography for the analysis of the fibrous microstructure of SMC composites. *Composites Part A: Applied Science and Manufacturing*. 2008;39(1):91-103.
- [2] Boylan S, Castro JM. Effect of reinforcement type and length on physical properties, surface quality, and cycle time for sheet molding compound (SMC) compression molded parts. *Journal of Applied Polymer Science*. 2003;90(9):2557-71.
- [3] Fitoussi J, Guo G, Baptiste D. A statistical micromechanical model of anisotropic damage for S.M.C. composites. *Composites Science and Technology*. 1998;58(5):759-63.
- [4] Wulfsberg J, Herrmann A, Ziegmann G, Lonsdorfer G, Stöß N, Fette M. Combination of Carbon Fiber Sheet Moulding Compound and Prepreg Compression Moulding in Aerospace Industry. *Procedia Engineering*. 2014;81:1601-7.
- [5] Feuilladea V, Bergereta A, Quantina J, Crespyb A. Characterisation of glass fibres used in automotive industry for SMC body panels. *Composites Part A: Applied Science and Manufacturing*. 2006;37(10):1536-1544.
- [6] Lu J, Khot S, Wool RP. New sheet molding compound resins from soybean oil. I. Synthesis and characterization. *Polymer*. 2005;46(1):71-80.
- [7] Oldenbo M, Fernberg SP, Berglund LA. Mechanical behaviour of SMC composites with toughening and low density additives. *Composites Part A: Applied Science and Manufacturing*. 2003;34(9):875-85.
- [8] Jendli Z, Meraghni F, Fitoussi J, Baptiste D. Multi-scales modeling of dynamic behaviour for discontinuous fibre SMC composites. *Composites Science and Technology*. 2009;69(1):97-103.
- [9] Dear JP, Brown SA. Impact damage processes in reinforced polymeric materials. *Composites Part A: Applied Science and Manufacturing*. 2003;34(5):411-20.
- [10] Jendli Z, Meraghni F, Fitoussi J, Baptiste D. Micromechanical analysis of strain rate effect on damage evolution in sheet molding compound composites. *Composites Part A: Applied Science and Manufacturing*. 2004;35(7-8):779-85.
- [11] Jendli Z, Fitoussi J, Meraghni F, Baptiste D. Anisotropic strain rate effects on the fibre-matrix interface decohesion in sheet moulding compound composites. *Composites Science and Technology*. 2005;65(3-4):387-93.
- [12] Fitoussi J, Meraghni F, Jendli Z, Hug G, Baptiste D. Experimental methodology for high strain-rates tensile behaviour analysis of polymer matrix composites. *Composites Science and Technology*. 2005;65(14):2174-88.
- [13] Le Corre S, Orgéas L, Favier D, Tourabi A, Maazouz A, Venet Cc. Shear and compression behaviour of sheet moulding compounds. *Composites Science and Technology*. 2002;62(4):571-7.
- [14] Naik NK, Yernamma P, Thoram NM, Gadipatri R, Kavala VR. High strain rate tensile behavior of woven fabric E-glass/epoxy composite. *Polymer Testing*. 2009;29(1):14-22.
- [15] Brown KA, Brooks R, Warrior NA. The static and high strain rate behaviour of a commingled E-glass/polypropylene woven fabric composite. *Composites Science and Technology*. 2009;70(2):272-83.
- [16] Jacob GC, Starbuck JM, Fellers JF, Simunovic S, Boeman RG. Strain rate effects on the mechanical properties of polymer composite materials. *Journal of Applied Polymer Science*. 2004;94(1):296-301.
- [17] Hsiao HM, Daniel IM. Strain rate behavior of composite materials. *Composites Part B: Engineering*. 1998;29(5):521-33.
- [18] Meraghni F, Desrumaux F, Benzeggagh ML. Implementation of a constitutive micromechanical model for damage analysis in glass mat reinforced composite structures. *Composites Science and Technology*. 2002;62(16):2087-97.
- [19] Fitoussi J, , Bocquet M, Meraghni F. Effect of the matrix behavior on the damage of ethylene-propylene glass fiber reinforced composite subjected to high strain rate tension. *Composites Part B: Engineering*. 2013;45(1): 1181-91.